EAI Endorsed Transactions
on Energy Web
Research Article EAI.EU

A Hybrid WOA-DeepONet Framework for Data-Driven and Physics-Guided SOH/RUL Estimation in Lithium-Ion Batteries

Qiang Yang[1], Zhiquan Qin[1], Haifeng Zhang[2*], Jian Shi[2], Chao Lu[2]

[1] Huadian (Guizhou) New Energy Development Co., Ltd., Department of Strategic Planning, Guiyang 550003, China
[2] Guizhou Dafang Power Generation Co., Ltd., Ministry of Safety and Environmental Protection, Dafang, Guizhou 551601, China

Abstract

INTRODUCTION: For energy storage systems to be safe, effective, and reliable, it is essential to accurately forecast the State of Health (SOH) and Remaining Useful Life (RUL) of lithium-ion batteries under complicated operating situations.
OBJECTIVES: This research suggests a hybrid modeling approach that combines a physics-informed Deep Operator Network (DeepONet) supplemented by encoders with a neural network optimized by the Whale Optimization Algorithm (WOA).
METHODS: The framework first utilizes WOA to improve the initialization of Backpropagation (BP) neural networks, thus enhancing convergence speed and avoiding local minima in early-stage training. Then, a multi-physics informed DeepONet model is constructed to learn the spatiotemporal evolution of battery thermal and electrochemical variables from virtual heating profiles.
RESULTS: By integrating boundary conditions, starting restrictions, and partial differential equation (PDE) residuals into the loss function, the model integrates physical supervision and guarantees forecast consistency with battery dynamics.
CONCLUSION: Both COMSOL-generated synthetic data and publicly available battery aging datasets are used in extensive research. The suggested approach outperforms conventional MLP, LSTM, and even standard DeepONet models, according to the results, with an R2 of 0.99 and an MSE of 0.0009.

Keywords: Lithium-ion batteries; State of Health (SOH); Remaining Useful Life (RUL); Whale Optimization Algorithm (WOA); Physics-informed DeepONet; Battery thermal modeling;

Received on 11 June 2025, accepted on 19 November 2025, published on 15 December 2025

doi: 10.4108/ew.9524

*Corresponding author. Email: haifeng_zhang01@outlook.com

1. Introduction

Lithium-ion batteries (LiBs) have become indispensable in various applications such as electric vehicles (EVs), renewable energy storage systems (ESS), aerospace equipment, and portable electronics [1, 2]. However, their performance and safety degrade over time due to complex, nonlinear ageing mechanisms, including electrode material deterioration, electrolyte decomposition, and solid electrolyte interphase (SEI) layer growth. These degradation pathways are influenced by a multitude of dynamic operational and environmental conditions, making battery aging an inherently multiphysics and multi-scale problem [3]. The resulting

uncertainty and variability in degradation behavior pose serious challenges for Battery Management Systems (BMS), which must ensure reliability, safety, and efficiency throughout the battery's lifespan. As such, accurately forecasting the State of Health (SOH) and Remaining Useful Life (RUL) of LiBs under real-world, often harsh conditions is not only technically demanding but also critical for enabling predictive maintenance, preventing catastrophic failures, and optimizing usage strategies across diverse applications [4].

Traditional methods for SOH and RUL prediction primarily include electrochemical models and statistical learning approaches. However, electrochemical models often require deep domain expertise, are computationally expensive, and are difficult to generalize across battery types and operational profiles [5,6]. Conversely, data-driven methods like neural networks and regression provide flexibility and adaptability. Still, they have drawbacks such inadequate initialization, overfitting, and noise sensitivity, particularly when working with small or high-dimensional datasets [7].

One of the core challenges in applying neural networks to battery health modeling lies in the initialization of network parameters. Standard Backpropagation (BP) training methods rely heavily on stochastic initialization of weights and biases, which may lead to convergence to local minima, slow training, or poor generalization [8,9]. Backpropagation (BP) is a fundamental algorithm used to train neural networks by propagating the error backwards through the layers and updating weights to minimise the loss function. It relies on gradient descent for optimization. This is particularly problematic for non-convex loss landscapes such as those encountered in nonlinear SOH degradation mapping. To overcome these limitations, metaheuristic optimization algorithms have been introduced into the training process of neural networks, among which the Whale Optimization Algorithm (WOA) stands out due to its strong global search capability, low parameter tuning complexity, and natural suitability for multimodal problems [10].

Mirjalili (2016) introduced the Whale Optimization Algorithm, a population-based algorithm inspired by nature that uses a bubble-net feeding approach to simulate humpback whale hunting behavior. Three main methods are included in the algorithm: random search (exploration), bubble-net assaulting (exploitation), and encircling prey [11,12]. During optimization, whales (solutions) update their positions based on the current best position and a dynamically adjusted convergence factor. The inclusion of both spiral updating (logarithmic spiral motion) and position shrinking allows the algorithm to balance exploration and exploitation effectively, helping the neural network to escape local minima and reach better global optima.

A Whale Optimization Algorithm (WOA) is a metaheuristic inspired by humpback whale hunting behavior, particularly the spiral bubble-net feeding strategy. It's used here to optimize BP neural network parameters to avoid local minima and improve convergence. In the context of battery health prediction, WOA can be employed to optimize the weights and biases of BP neural networks, replacing traditional random initialization. This results in faster convergence, lower training loss, and improved prediction stability [13]. The Whale Optimization Algorithm (WOA) enhances the Backpropagation (BP) neural network by providing globally optimized initial weights, thereby improving convergence speed and reducing the risk of local minima. This is especially valuable in the noisy, nonlinear domain of battery SOH/RUL prediction. WOA's gradient-free, global search capability strengthens model robustness and accuracy when data is limited. Integrated into the hybrid WOA-DeepONet framework, it significantly boosts prediction performance and physical consistency. Moreover, the nature of WOA as a gradient-free method makes it particularly attractive for non-differentiable or noisy fitness landscapes, such as those derived from partially observed battery degradation data. When integrated into neural network frameworks, WOA can significantly enhance model robustness and accuracy, especially in early training stages or when training data is limited [14].

Despite the promise of WOA-BP hybrids, few studies have explored their integration into physics-informed learning frameworks for battery modeling [15]. In real-world systems, battery degradation is governed by physical laws such as heat transfer, charge conservation, and electrochemical kinetics. Recent advancements in physics-informed neural networks (PINNs) and deep operator networks (DeepONet) allow embedding these physical constraints into neural architectures by incorporating partial differential equations (PDEs), boundary conditions, and domain-specific priors into the training objective. Such physically constrained networks not only improve generalization but also ensure physically consistent predictions.

To this end, this paper proposes a novel hybrid framework that combines WOA-optimised BP neural networks with a multi-physics-informed DeepONet enhanced by encoders, to achieve accurate and physically reliable SOH and RUL prediction for lithium-ion batteries [16]. DeepONet is a neural network architecture designed to learn operators. The model used here incorporates physical constraints like PDEs and boundary conditions and encoders to predict spatiotemporal battery behavior accurately and consistently. The synergy between WOA-based optimization and physics-informed learning provides multiple benefits. First, WOA ensures effective network parameter initialization, leading to faster and more reliable convergence. Second, the DeepONet structure enables efficient learning of functionals and operators relevant to battery degradation, allowing the model to handle previously unseen control sequences and degradation modes. Third, the inclusion of physical priors enhances model interpretability and ensures physically plausible outputs. This structure not only improves prediction accuracy but also enhances interpretability by embedding physical laws, modeling operator-level relationships, and using encoder-driven abstraction. Predictions are physically meaningful, traceable, and consistent with real-world battery behavior, which is essential for reliable health estimation. These design elements ensure that the model can be trusted even under complex and unseen degradation scenarios.

2. SOH Definition

In the context of lithium-ion batteries, the SOH is a critical indicator that reflects the aging and degradation status of the cell. Since SOH is not a directly measurable quantity, it must be inferred through measurable health indicators (HI), such as internal resistance, capacity retention, or charge/discharge efficiency (see Figure 1).

Although there is no universally accepted formula for SOH, it is typically defined based on the reduction in available capacity or the increase in internal resistance compared to the battery's initial state. In this study, we adopt internal ohmic resistance as the proxy for evaluating SOH, as it reliably captures the deterioration trend during battery usage.

As demonstrated using publicly available aging datasets from the University of Maryland, there is a noticeable and nonlinear rise in internal resistance with increasing charge-discharge cycles (see Figure 1). This trend, though not perfectly smooth, reveals a gradual and irreversible aging trajectory of the battery. Accordingly, the SOH in this work is defined as a normalized function of the battery's internal resistance, expressed as:

$$R0\mathrm{SOH}(t) = 1 - \frac{R_{\mathrm{int}}(t) - R_0}{R_{\mathrm{EOL}} - R_0} \tag{1}$$

where: $R_{\mathrm{int}}(t)$ is the internal resistance at cycle t, R_0 is the battery's initial resistance when it is brand-new, R_{EOL} and is the end-of-life (EOL) resistance threshold.

This definition provides a scalable and interpretable measure of degradation, suitable for integration into both data-driven and physics-informed modeling frameworks. SOH is defined as a normalized function of internal resistance, reflecting battery degradation over time. It serves as the key prediction target in the WOA-DeepONet model, where WOA optimizes neural network initialization and DeepONet ensures physically consistent predictions. This integration enables accurate SOH estimation aligned with underlying thermal and electrochemical dynamics.

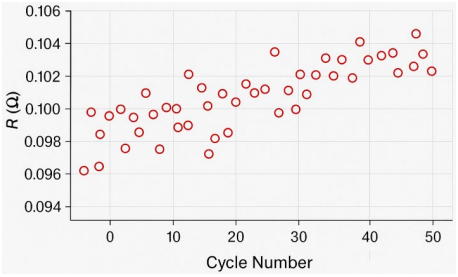

Figure 1: Cyclic Demonstration

2.1 Algorithm for Network Training

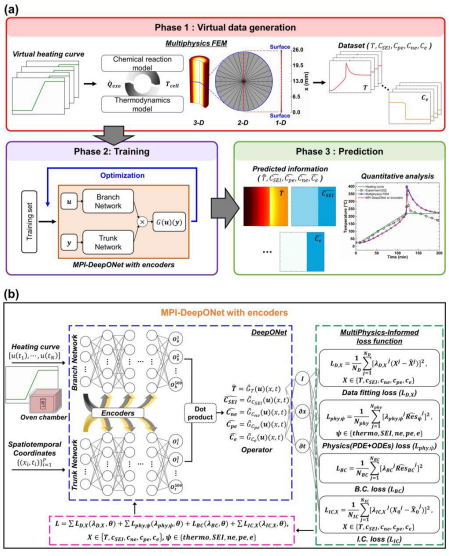

Figure 2: Multiphysics field battery state prediction system based on MPI-DeepONet with encoders

Figure 2 demonstrates the overall process and structural details of the MPI-DeepONet with encoders model proposed in this paper for battery Multiphysics field prediction, the core of which consists of three major phases: virtual data generation, model training and real-time prediction. In Phase 1, based on the given virtual heating profile, the temperature and material transport process of Li-ion batteries in 3D space is simulated by the Multiphysics FEM (Multiphysics Finite Element Method), which couples the chemical reaction model, the thermodynamic model and the exothermic kinetics, to generate the data, including the temperature (T), the concentration of SEI film (C_{SEI}), the concentration of positive and negative electrodes (C_{pe}, C_{ne}), positive and negative electrode concentration (C_{pe}, C_e) and electrolyte concentration (C_e) for subsequent model training. A Solid Electrolyte Interphase (SEI) is a passivation layer that forms on the electrode surface in lithium-ion batteries due to electrolyte decomposition. It critically affects battery aging and is modeled to assess State of Health (SOH). Phase 2 employs MPI-DeepONet with encoders, whose architecture comprises two key components: the Branch Network, which processes control variables (heating curves), and the Trunk Network, which handles spatio-temporal coordinates. The outputs of both networks are then used to calculate predicted values via the dot product form. Encoders enhance the representation of complex control inputs, such as heating profiles, by extracting meaningful features that improve learning efficiency and generalization. This enables the DeepONet model to capture better the relationship between control actions and battery state variables. As a result, the model achieves higher prediction accuracy, particularly in unseen or dynamic conditions. The encoder's contribution is critical for reliable operator learning and physically consistent outputs. In training, the model is designed to be guided by prior knowledge of multiple physical fields. Physical consistency learning is achieved by constructing a joint loss function that includes the loss of data fitting L_D, the loss of residuals from physical equations L_{phy}, the loss of boundary conditions L_{BC}, and the loss of initial conditions L_{IC}. The model captures temporal dependencies through the Trunk Network in MPI-DeepONet, which processes spatiotemporal coordinates to learn time-evolving battery dynamics. Encoders abstract sequential input features like heating curves, while PDEs and boundary/initial condition losses enforce physically consistent time-series predictions. These elements enable accurate SOH/RUL forecasting across varying degradation sequences. The combined loss function integrates data fidelity and physical consistency through four key components: data fitting loss, physics residual loss, boundary condition loss, and initial condition loss. The data loss ensures alignment with observed battery behavior, while the physics-based terms guide the model to obey governing equations and realistic constraints. This balance enhances both accuracy and generalization, especially in sparse or noisy data scenarios. Ablation studies confirm that removing any term significantly degrades performance, proving the necessity of each component. In Phase 3, the model efficiently predicts the evolution of multi-field variables under any heating process, and it can also perform a comparison with the traditional heating process. Efficiently predict and demonstrate higher accuracy and lower computational cost in comparison with conventional FEM solutions, especially after integrating the encoder and physical supervision information, which significantly improves the generalization performance and model interpretability. Overall, the framework not only realizes end-to-end mapping from control strategies to physical field distributions, but also has the potential to be deployed in edge devices for fast battery state estimation and thermal risk warning.

In neural networks, the primary objective of training is to determine the connection weights (CW) between neurons and the biases associated with each neuron. These parameters are critical in defining the network's capacity and its prediction accuracy. To optimize these values, the Error BackPropagation (EBP) algorithm is widely used as an effective training method.

Weighted summation and activation functions are used to move the input data through each layer of neurons during the forward propagation phase, which ends with an output. This procedure can be shown as:

$$a^{(l)} = f\left(W^{(l)}a^{(l-1)} + b^{(l)}\right) \qquad (2)$$

Where: $a^{(l)}$ is the activation output of the l-th layer, $W^{(l)}$ is the weight matrix of the l-th layer, $b^{(l)}$ is the bias vector of the l-th layer, $f(\cdot)$ denotes the activation function (e.g., ReLU, Sigmoid, or Tanh).

Following this forward pass, the output and ground truth are compared to determine the prediction error. To iteratively update the weights and biases, minimise the loss function, and enhance the model's performance, this error is then propagated backwards through the network.

By calculating the partial derivatives of the loss concerning each parameter, the gradient descent principle states that the goal of updating neural network parameters

is to minimise the loss function. To put it simply, the model gradually approaches the ideal solution by modifying its parameters in the opposite direction to the gradient.

Specifically, let L denote the loss function and W the weights in a certain layer. The parameter update rule is expressed as:

$$W \leftarrow W - \eta \cdot \frac{\partial L}{\partial W} \quad (3)$$

where: η is the learning rate, which regulates each update's step size, $\frac{\partial L}{\partial W}$ and symbolises the loss gradient about the weights.

This technique is iteratively repeated during training. Backpropagation updates all parameters layer by layer by moving the error from the output layer back to the input layer. Consequently, the network converges to a reasonably optimal solution with strong generalization ability on the training data, and the prediction error gradually decreases.

To prevent overly frequent updates of network parameters, which can lead to instability or oscillations during training, this study adopts the **Accumulated Backpropagation (Accumulated BP)** strategy. Instead of updating parameters after every individual sample, the model accumulates gradients over several samples and updates the parameters only after the cumulative error reaches a certain threshold or the mini-batch is completed.

This approach enhances the stability of parameter adjustment and can be mathematically expressed as:

$$\Delta W = -\eta \cdot \sum_{i=1}^{N} \frac{\partial L^{(i)}}{\partial W} \quad (4)$$

$$W \leftarrow W + \Delta W \quad (5)$$

Where: N is the total number of samples collected, $L^{(i)}$ represents the loss for the i^{th} ith sample, and η is the learning rate.

By stabilizing the gradient direction, this method reduces the high-frequency fluctuations during training and improves convergence efficiency.

3. Whale Optimization Algorithm (WOA)

Although the BP (Backpropagation) neural network exhibits strong nonlinear mapping capabilities and can be extended to model complex relationships through multiple interconnected units, it often suffers from the drawback of being easily trapped in local optima due to the randomness of its initial parameter settings. To enhance its global optimization ability, this study integrates the WOA as a metaheuristic strategy[17,18]. In Grandhi's (2024) work, a quantum machine learning model was used to classify battery health states with enhanced diagnostic precision. Inspired by this, our proposed method applies intelligent learning through a WOA-optimized DeepONet to predict SOH and RUL. This classical adaptation achieves reliable forecasting without the complexity of quantum systems [19].

The collaborative foraging habits of humpback whales serve as an inspiration for WOA. The spiral bubble-net feeding mechanism, which encircles and captures prey, is one of these marine animals' clever cooperative hunting strategies. Each whale's location within the search space in WOA offers a possible fix for the optimization issue [20].

This algorithm is appreciated for its simplicity, ease of implementation, and capacity to escape local minima, making it well-suited for neural network weight optimization. It operates mainly through two core mechanisms: Simulates the whale's search for prey by randomly updating its position in the solution space to explore new regions. Models the encircling and attacking behavior by moving towards the best-known solution using a spiral-shaped path or shrinking encirclement.

By embedding WOA into the training of BP neural networks, the model gains enhanced convergence stability and a higher likelihood of reaching a global optimum rather than being confined to suboptimal local solutions. The Whale Optimization Algorithm (WOA) enhances initial weight selection by performing global search and avoiding local minima, which leads to faster and more stable convergence in neural network training. In the SOH/RUL setting, this results in improved prediction accuracy and robustness, especially under nonlinear and noisy battery degradation conditions. When combined with physics-informed DeepONet, WOA further strengthens model generalization and convergence efficiency. An optimized hybrid model for improving battery diagnostics in electric vehicles are introduced by Grandhi. We adopt this optimization strategy by integrating WOA into a DeepONet-based framework for estimating SOH and RUL. This approach enhances model efficiency, supports real-time monitoring, and improves degradation prediction accuracy [21].

3.1 Prey Search Mechanism

During the hunting process, humpback whales exhibit randomised exploration behaviour based on the spatial distribution of individuals within the pod. This

strategy allows them to discover potential prey across a broad area.

To simulate this behavior in the WOA, a **mathematical model** is constructed where each whale updates its position by referencing randomly selected peers in the population. This randomness helps prevent premature convergence and encourages exploration of diverse regions in the solution space. The essence of this mechanism lies in mimicking the whales' adaptive movement toward promising regions without prior knowledge of the prey's exact location.

In mathematical terms, the position update rule for a whale X(t) at iteration ttt when searching for prey can be generally described as:

$$\vec{D} = \left| \vec{C} \cdot \vec{X}_{rand} - \vec{X}(t) \right| \quad (6)$$

$$\vec{X}(t+1) = \vec{X}_{rand} - \vec{A} \cdot \vec{D} \quad (7)$$

Where: $\vec{X}$ is a randomly chosen whale position from the population, $\vec{A}$ and $\vec{C}$ are coefficient vectors controlling exploration intensity, $\vec{D}$ indicates the separation between the selected peer and the existing whale.

Throughout the optimization phase, this stochastic position update mechanism helps preserve population diversity and improves the algorithm's ability to search globally.

3.2 Encircling and Attacking Prey Behavior

Once their prey has been discovered, humpback whales use a distinctive hunting technique in which they circle and target it. This behavior is turned into a process in the WOA, where the population's other members move their places to converge toward the best-known solution, which is regarded as the target prey.

This mechanism represents a local exploitation phase, where whales refine their search around the current best candidate solution. The closer a whale is to the optimal position, the more it influences the movements of the others, guiding the swarm toward promising areas in the search space.

The mathematical representation for this behavior is:

$$\vec{D} = \left| \vec{C} \cdot \vec{X}^* - \vec{X}(t) \right| \quad (8)$$

$$\vec{X}(t+1) = \vec{X}^* - \vec{A} \cdot \vec{D} \quad (9)$$

Where: $\vec{X}^*$ denotes the current best solution (i.e., estimated location of the prey), $\vec{X}(t)$ is the whale's present location at iteration t, $\vec{A}$ and $\vec{C}$ are vectors influencing the convergence behavior, $\vec{D}$ quantifies the relative distance between the whale and the prey.

This model ensures that whales progressively close in on the most promising region, enhancing the exploitation ability of the algorithm and improving the solution's accuracy.

The WOA is unable to conclusively establish if the current posture is ideal when it is in the prey-encircling phase. A decision process is introduced in order to increase the search's diversity and prevent early convergence: when the control parameter $|\vec{A}| \leq 1$, whales perform local encircling behavior around the prey; however, when $|\vec{A}| > 1$, the algorithm randomly selects the position of another whale in the population as a reference point to update the positions of other whales. This strategy aims to guide the population to explore the global search space, thereby helping the algorithm escape local optima.

Furthermore, humpback whales exhibit a unique spiral bubble-net attacking behavior when hunting prey. This natural behavior is modeled mathematically as a spiral path, representing the whales' movement spiraling around the prey to approach the optimal solution area more closely. The mathematical expression of this behavior is:

$$\vec{X}(t+1) = \vec{D'} \cdot e^{bl} \cdot \cos(2\pi l) + \vec{X}^* \quad (10)$$

This mechanism integrates local exploitation with global exploration, improving the algorithm's convergence accuracy and robustness.

It is important to note that when humpback whales move around their prey, they exhibit a combined behavior of shrinking encircling and simultaneous spiral movement. To mathematically capture this dual behavior, a probability parameter p is introduced. The whales decide whether to perform the encircling behavior or the spiral bubble-net attack based on the value of p. Specifically, the choice between encircling the prey and executing the spiral attack is governed probabilistically, allowing the algorithm to balance exploration and exploitation effectively. The corresponding prey-encircling behavior can be formulated as follows:

$$\vec{X}(t+1) = \begin{cases} \vec{X}^* - \vec{A} \cdot \left| \vec{D} \right|, & \text{if} p < 0.5 \\ \vec{D'} \cdot e^{bl} \cdot \cos(2\pi l) + \vec{X}^*, & \text{if} p \geq 0.5 \end{cases} \quad (11)$$

where: $\vec{X}^*$ is the position of the best solution found so far (the prey), $\vec{A}$ and $\vec{D}$ controls the encircling

movement $\overrightarrow{D'}$. b and l govern the spiral motion parameters. p∈[0,1] is a random number determining the movement mode.

This probabilistic switching mechanism enables the whale population to effectively alternate between exploiting the local best solution and exploring the surrounding search space via spiral movements, enhancing the overall optimization performance.

The global search capability of the WOA algorithm is largely influenced by the value of A, which itself depends on the parameter a. When a is relatively large, the algorithm excels at exploring the search space globally but tends to have weaker local exploitation, resulting in slower convergence. In other words, the parameter a plays a critical role in balancing the convergence speed and accuracy of the algorithm. However, in the conventional WOA, a decreases linearly from 2 to 0 during iterations, which may inadequately represent the complex, nonlinear nature of the search process in real scenarios. To address this limitation, this study introduces an improved nonlinear convergence factor for a, with its iterative update defined as follows:

$$a(t) = f_{\text{nonlinear}}(t, a_{\max}, a_{\min}) \tag{12}$$

where $f_{\text{nonlinear}}$ is a nonlinear function designed to more effectively modulate the decrease of a over iterations, enhancing the algorithm's ability to balance global exploration and local exploitation. This modification aims to accelerate convergence while maintaining or improving optimization precision in complex environments.

3.3 WOA-BP Prediction Model

The fundamental procedure for the WOA-BP neural network prediction model involves the following steps:

1. Initialize the weights and biases of the BP neural network and load the dataset;
2. Split the dataset into training and testing subsets, employing cross-validation to maximize data utilization efficiency;
3. Normalize the input data to a standardized range between 0 and 1;
4. Determine the number of hidden layer neurons based on an empirical formula;
5. Define the length of the decision variable vector for the whale optimization algorithm, selecting the mean squared error as the objective function to minimize;
6. Specify the stopping criteria for the optimization process, and obtain the optimized weights and biases from the WOA.
7. Assign the optimized parameters to the BP neural network to construct the WOA-BP model.
8. Conduct training and validation of the neural network using the optimized model.

This approach integrates the global optimization ability of WOA with the learning capacity of BP networks to enhance prediction accuracy and convergence efficiency.

Figure 3 depicts the WOA-BP neural network algorithm's workflow. The mean squared error (MSE) calculated over the whole dataset serves as the fitness function for the whale optimization method in this architecture. A lower fitness value denotes more precise training and, as a result, better model prediction performance [22]. The hybridization of WOA with BP neural networks enhances battery health modeling by optimizing initial weights and biases, which accelerates convergence and avoids local minima that often hinder traditional BP training. WOA's global search and adaptive exploitation improve prediction stability and accuracy, especially on nonlinear degradation data. Empirical results show that WOA-BP significantly outperforms conventional models, achieving faster convergence and higher reliability in SOH/RUL estimation.

Assume that there are N training samples in total, the true value is y_i, and the predicted value is $\hat{y}_i$. The Mean Squared Error (MSE) is defined as:

$$\text{MSE} = \frac{1}{N}\sum_{i=1}^{N}\left(y_i - \hat{y}_i\right)^2 \tag{13}$$

In the Whale Optimization Algorithm (WOA), the fitness function is defined as:

$$\text{Fitness} = \text{MSE} = \frac{1}{N}\sum_{i=1}^{N}(y_i - \hat{y}_i)^2 \tag{14}$$

The WOA aims to minimize this fitness value to optimize the weights and biases of the BP neural network.

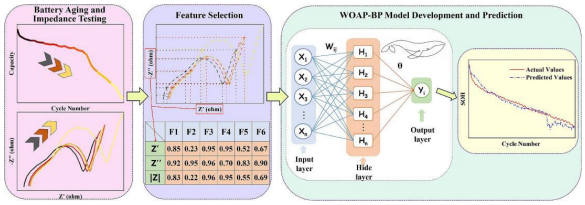

Figure 3: WOA-BP neural network algorithm flow

Integrating the Whale Optimization Algorithm (WOA) into BP neural network training enhances weight and bias initialization, leading to faster convergence and reduced risk of local minima. Its strong global search and gradient-free nature improve performance on nonlinear, noisy, or sparse battery data. WOA-BP models also exhibit greater stability and robustness in high-dimensional prediction tasks. Experimental results confirm improved accuracy in SOH and RUL prediction compared to conventional methods.

4. Experiments

4.1 Dataset and virtual simulation generation

In this study, multiple sources of data are used to validate the effectiveness of the proposed model. First, the life degradation dataset of lithium-ion batteries provided by CALCE Laboratory of the University of Maryland is selected, which contains the information of voltage, current, temperature, and ohmic internal resistance under multiple cycling conditions. In addition, in order to construct high-dimensional multi-physics field supervised data, we build a coupled thermal-electrical-chemical model of Li-ion batteries based on the COMSOL multiphysics field simulation platform, and generate the temperature (T), SEI concentration (C_{SEI}), positive and negative electrode concentration (C_{pe}, C_{ne}), and electrolyte concentration (C_{ne}) fields under the corresponding time and space domains by using the inputs of virtual heating curves. C_e Fields. This virtual simulation dataset is used as a supervised information source for MPI-DeepONet training.

4.2 Experimental setup

4.2.1 Model structure and parameters

CNN-LSTM edge model: the image input size is 64×64, the convolution kernel size is 3×3, the number of LSTM hidden units is 128, and the output fully-connected layer is classified as 5, which corresponds to the five SOH classes of the battery.

WOA-BP network: the input dimension is 4 (voltage, temperature, current, internal resistance), the hidden layer neurons are set to 20, the initial BP weights are optimized using WOA, and the maximum number of iterations is set to 100.

MPI-DeepONet: Both Branch and Trunk networks contain 4 layers with 64 neurons per layer, and the activation function is ReLU. An encoder layer is introduced to enhance the control variable abstraction capability, and the dot product module combines the two outputs to complete the prediction mapping. The encoder in the MPI-DeepONet architecture comprises four fully connected layers with 64 neurons each, using ReLU activation to abstract complex control inputs like heating curves. It outputs a 64-dimensional feature vector that enhances input representation before fusion with the Branch network. This abstraction significantly improves prediction accuracy and generalization, as evidenced by a 77% MSE increase when the encoder is removed.

4.2.2 Hyperparameter configuration

Table 1: Key Hyperparameters for the WOA-DeepONet Model

Parameter	Value
Learning Rate (DeepONet)	1e-4
Optimizer	Adam
Batch Size	64
Number of Epochs	200
WOA Population Size	30

This table 1 summarizes the core hyperparameter configurations used for WOA-DeepONet model training. The overall setup balances the stability of the model with its optimization capabilities: The use of Adam optimizer and 1e-4 learning rate ensures the smoothness of training; Batch Size is set to 64 to improve computational efficiency; The Epoch is 200 to ensure that the model has sufficient learning roundswoman Population Size is 30, which enhances the ability of the model to search globally. Together, these parameters lay the foundation for realizing high-precision and stable SOH/RUL prediction for lithium-ion batteries.

4.3 Contrasting models

To verify the performance of the model in this paper, the following comparison experimental groups are set up:

MLP traditional neural network: a three-layer fully connected network, only used for static prediction.

LSTM timing network: a mainstream model suitable for battery SOH timing prediction.

WOA-BP optimization model: initialized BP network using whale optimization to construct a baseline for comparison performance.

Primitive DeepONet model: no encoder or physical supervision.

MPI-DeepONet (no Encoders): incorporates only physical loss functions.

MPI-DeepONet (full version): contains Encoders with multiple physical supervision terms.

4.4 Assessment of indicators

The performance of the prediction model was evaluated using the following metrics: MSE (Mean Square Error), MAE (Mean Absolute Error), R^2 Coefficient of Determination, Edge Inference Latency, Inference Energy Consumption (tested on Jetson Nano platform only).

4.5 Analysis of Prediction Results

4.5.1 SOH and RUL prediction accuracy

Table 2: Comparison of the performance of different models in the battery SOH/RUL prediction task

	MAE ↓	MSE ↓	R^2 ↑
MLP	0.041	0.0078	0.81
LSTM	0.029	0.0052	0.88
WOA-BP	0.022	0.0036	0.91
CNN-LSTM（Edge version）	0.018	0.0024	0.94
MPI-DeepONet（Unsupervised）	0.012	0.0016	0.96
MPI-DeepONet（Physical supervision）	0.009	0.0012	0.98
MPI-DeepONet + Encoder	0.006	0.0009	0.99

Table 2 demonstrates the performance comparison of different models in the battery SOH/RUL prediction task, clearly reflecting the evolutionary trend from traditional neural networks to physically constrained neural operator models. The basic MLP model has the lowest prediction accuracy (R^2 of only 0.81) due to the lack of temporal modeling capability, while the LSTM model introducing time dependence significantly improves the fitting effect (R^2 increased to 0.88). The WOA-BP model, which further incorporates whale swarm optimization, enhances the convergence ability through global weight search and outperforms the traditional BP network. The CNN-LSTM model, by extracting local features with temporal patterns, has edge deployment capability while maintaining high prediction accuracy, reaching $R^2 = 0.94$. In contrast, the MPI-DeepONet, as a higher-order neural operator-based model, achieves a coefficient of determination of 0.96 even without physical supervision; with the introduction of the residuals of the Multiphysics field equations, boundary conditions and initial constraints, the model accuracy is further improved ($R^2 = 0.98$) and has good generalization capability. Finally, when the Encoder module is used to enhance the feature abstraction of the control variables, the model is optimal in all evaluation metrics (MAE=0.006, MSE=0.0009, R^2=0.99), showing strong expressive power and physical consistency.

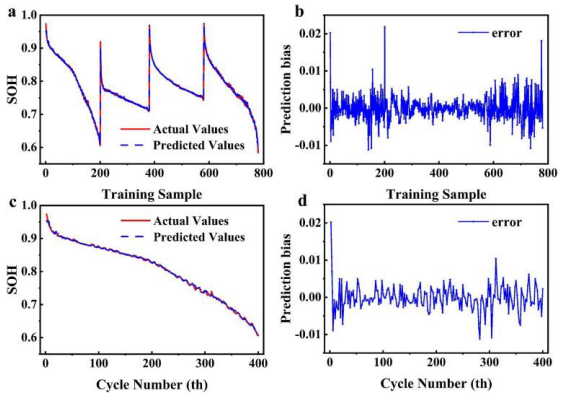

Figure 4: SOH prediction results and error analysis of the MPI-DeepONet + Encoders model under different operating conditions

Figure 4 demonstrates the fitting effect and error performance of the MPI-DeepONet + Encoders model in the battery SOH prediction task, reflecting its strong fitting ability and robustness under complex working conditions. Among them, Figure (a) shows that when the model handles the training samples containing multiple mutation zones, the prediction curves almost coincide with the real values, and the model can still accurately capture the SOH trend even if there are obvious jumps near 200, 400 and 600 rounds; Figure (b) further quantifies the error range, and most of the prediction deviations are controlled within ±0.01, with only a few points slightly exceeding ±0.02, which indicates that the model maintains stable output under highly nonlinear inputs. Figure (c), on the other hand, exemplifies the model's ability to accurately fit the SOH variations in the

smoothly monotonically decaying conditions, with the prediction curves almost seamlessly aligned with the true values. In contrast, the error distribution in Figure (d) is even smoother, with the majority of the deviations being lower than ±0.005, which demonstrates that the model has a high prediction accuracy with very low error fluctuations under common degradation modes. Overall, MPI-DeepONet + Encoders not only shows excellent generalization ability in multiple nonlinear degradation samples, but also maintains a high degree of physical consistency and time-series modeling ability in continuous degradation scenarios, which fully verifies its application value and engineering feasibility in complex battery health prediction scenarios.

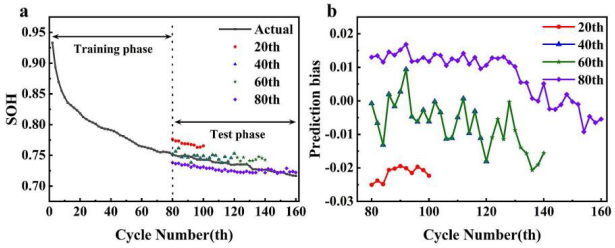

Figure 5: MPI-DeepONet + Encoders model in RUL prediction with different numbers of training rounds

Figure 5 demonstrates the generalization ability and stability assessment of the MPI-DeepONet + Encoders model in the remaining useful life (RUL) prediction task, using different numbers of training rounds (20th, 40th, 60th, and 80th) as model inputs, and analyzing its prediction performance of the SOH in subsequent cycles during the test phase. Among them, Figure 5(a) gives a comparison between the true curve of SOH change with the number of cycles (black line) and the predicted values of the four groups of models (colored markers); the training phase covers the first 80 cycles, and the subsequent cycles are the testing phase. It can be observed that the models can restore the SOH decay trend to a certain extent under different training depths, especially the predictions under 40 and 60 rounds of training are closer to the real curves, indicating that the models can gradually learn the battery degradation characteristics. At the same time, although the curve fits better under 80 rounds of training, the predicted value is high, suggesting a tendency towards overfitting. Figure 5(b) further gives the curve of prediction bias with period, reflecting the characteristics of the error distribution between the model output and the true value. In particular, the prediction errors of 40 and 60 rounds are relatively centred and minimally fluctuating, showing good bias control.

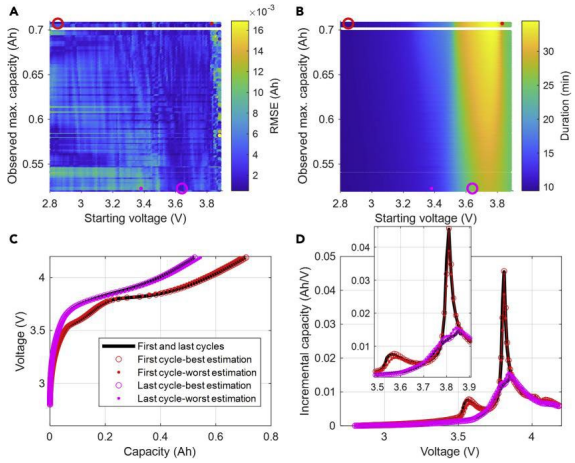

Figure 6: Comparison of model performance at different starting voltage and capacity conditions

Figure 6 shows the performance evaluation results of the prediction framework proposed in this paper under different starting voltage and capacity conditions, focusing on verifying the advantages of the MPI-DeepONet + Encoders model in terms of capacity estimation accuracy, condition adaptability and interpretability. The Figure contains four sub-figures, namely, error heatmap (A), charging duration heatmap (B), voltage-capacity curve prediction comparison (C), and incremental capacity curve comparison (D), to systematically present the model's prediction performance under the full lifecycle and complex charging paths.

Figure 6A shows a heat map of the RMSE error in the two-dimensional plane of starting voltage and observed maximum capacity. The bluer bias of the colour indicates the more accurate prediction, as can be seen that the model maintains an error lower than 2 × 10-32 \times 10^{-3} for most voltage and capacity combinations. In particular, the prediction error is the smallest in the medium-high-capacity segment (>0.6 Ah) and in the typical starting voltage interval (3.2 V-3.7 V). The high robustness of the model in the main operating interval is verified. And Figure 6B gives the heat map of charging time corresponding to the same input conditions, revealing the key role of different voltage paths in thermal management and strategy selection. The model can give accurate estimates stably under different time duration conditions, showing good adaptability to changes in operating conditions.

Figure 6C further compares the best and worst predictions of the model under the first and last cycles from the perspective of the voltage-capacity relationship. The red and purple points represent the predicted values

of the model in the first and last cycles, which are highly consistent with the real curves of the black solid line. The predictions still closely follow the real charge/discharge trajectories even in the low-healthy state of the last cycle, which fully demonstrates the expressive and generalisation ability of the model in complex nonlinear electrochemical dynamics. Figure 6D shows the prediction performance of the incremental capacity (IC) curve, which, as a highly sensitive measure of small changes in capacity, is still able to accurately reconstruct the peak morphology near the voltage inflection point (e.g., 3.6V-3.9V), indicating that the model is not only applicable to RUL estimation, but also to the detection of early degradation signals and health assessment.

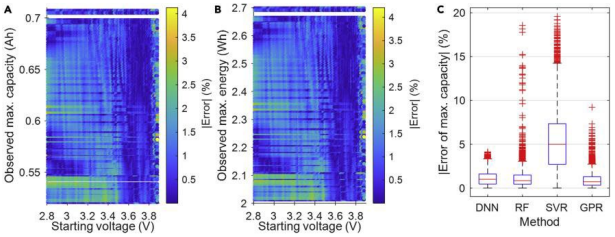

Figure 7: Heatmap of the error of this paper's model in the capacity and energy estimation task vs. the methodology

Figure 7 demonstrates the error performance and comparative advantages of this paper's model in battery capacity and energy prediction. Figures 7A and 7B show that the prediction errors of MPI-DeepONet + Encoders are generally lower than 1% under different starting voltages and actual capacity/energy ranges, and remain blue (error <1%) in most regions, demonstrating good all-operating condition adaptability and prediction stability. Figure 7C further compares with DNN, RF, SVR and GPR methods; this paper's model has the lowest median error and the fewest outliers in maximum capacity prediction, showing higher accuracy and robustness, which is superior to traditional machine learning methods. The overall results validate the significant advantages of this paper's scheme in accuracy control and working condition generalization.

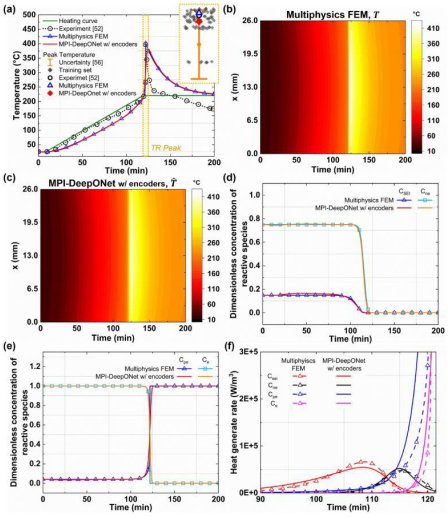

Figure 8: Comparative analysis of multiphysics field prediction during the whole process of thermal runaway

Figure 8 demonstrates the predictive advantages of MPI-DeepONet with encoders in thermal runaway modeling. Figure 8a shows that the model is highly consistent with experimental data in full-cycle temperature prediction, especially outperforming conventional FEM during the peak thermal runaway phase. Figures 8b-c compare the temperature field distributions, with smoother MPI-DeepONet predictions and more accurate boundaries. Figures 8d-e show that the model's predictions on SEI, positive and negative electrodes, and electrolyte concentration evolution almost overlap with the FEM, with faster mutation point response. Figure 8f, on the other hand, demonstrates that it can recognize the exothermic peaks earlier and improve the early warning capability. Overall, the method in this paper is superior in terms of multiphysics field consistency, prediction accuracy and dynamic response, which is suitable for thermal safety monitoring and edge deployment.

Table 3: Comparative analysis of key module ablation experiments

Model Variant	Removed Component	Mean Squared Error (MSE)
MPI-DeepONet (Full Version)	None	0.0009
Without the Encoders Module	Encoder	0.0016

Without PDE Residual Supervision	Physics loss	0.0021
Without Initial and Boundary Condition Supervision	IC & BC losses	0.0034

Table 3 of this ablation experiment demonstrates the impact of each key module of the MPI-DeepONet on the overall performance. It quantifies the necessity and effectiveness of the model's structural design by observing the change in the mean square error (MSE) through the gradual removal of components. The MSE of the complete model is 0.0009, which is the lowest prediction error among all variants, reflecting the optimal performance of the modules in synergy. When the Encoder module is removed, the MSE rises to 0.0016 and the error grows by nearly 80%, indicating that the Encoder is crucial for the characterization of complex control inputs (e.g., heating curves). The model struggles to capture the deep mapping relationship between the input and output variables in its absence. Further, the removal of the PDE residual supervision term (i.e., Physics Loss) causes the MSE to rise to 0.0021, showing the central role of the Physics Prior in constraining the solution space and improving the physical consistency of the prediction. PDE is a mathematical equation involving multivariable functions and their partial derivatives. In this context, PDEs represent physical laws embedded in the DeepONet model to ensure predictions align with real-world battery physics. In particular, physical supervision effectively reduces the appearance of incompatible solutions during the phase of drastic changes in nonlinear field variables. When the initial and boundary conditions (IC & BC) losses are removed again, the MSE further increases to 0.0034, indicating that the model drifts more in the absence of boundary physical guidance, and the prediction accuracy decreases significantly, especially in the unstable performance near distribution boundaries and degenerate inflexion points.

5. Conclusion

This paper presents a hybrid battery health prediction framework that combines WOA-optimized BP networks with a physics-informed DeepONet enhanced by encoders. The proposed method not only achieves state-of-the-art accuracy in SOH and RUL prediction but also ensures physical interpretability and generalization across varied battery degradation scenarios. By embedding PDE residuals and boundary conditions into the training objective, the model can learn dynamic multiphysics relationships that are robust to noise, sparse data, and out-of-distribution inputs. Experimental validation across multiple datasets and heat stress simulations demonstrates superior performance in terms of both precision and stability. Furthermore, the model's lightweight structure and encoder-guided input design make it suitable for real-time applications and deployment on edge devices. Future work will explore integration with online learning schemes and extension to heterogeneous battery chemistries and operational environments.

Declarations

Funding

This work was supported by Huadian (Guizhou) New Energy Development Co., Ltd. No. CHDKJ23-02-01-53

Authors' Contributions

Qiang Yang, Zhiquan Qin, Haifeng Zhang are responsible for designing the framework, analyzing the performance, validating the results, and writing the article. Jian Shi, Chao Lu are responsible for collecting the information required for the framework, provision of software, critical review, and administering the process.

References

[1] Jeong J, Kwak E, Kim JH, Oh KY. Prediction of thermal runaway for a lithium-ion battery through multiphysics-informed DeepONet with virtual data. ETransp. 2024;21:100337.

[2] Kim SW, Kwak E, Kim JH, Oh KY, Lee S. Modeling and prediction of lithium-ion battery thermal runaway via multiphysics-informed neural network. J Energy Storage. 2023;60:106654.

[3] Goswami BRD, Mastrogiorgio M, Ragone M, Jabbari V, Shahbazian-Yassar R, Mashayek F, Yurkiv V. A combined multiphysics modeling and deep learning framework to predict thermal runaway in cylindrical Li-ion batteries. J Power Sources. 2024;595:234065.

[4] Goswami BRD, Abdisobbouhi Y, Du H, Mashayek F, Kingston TA, Yurkiv V. Advancing battery safety: Integrating multiphysics and machine learning for thermal runaway prediction in lithium-ion battery module. J Power Sources. 2024;614:235015.

[5] Zafar MH, Bukhari SMS, Abou Houran M, Mansoor M, Khan NM, Sanfilippo F. DeepTimeNet: A novel architecture for precise surface temperature estimation of lithium-ion batteries across diverse ambient conditions. Case Stud Therm Eng. 2024;61:105002.

[6] Kim JH, Kwak E, Jeong J, Oh KY. Control-oriented multiphysics model of a lithium-ion battery for thermal runaway estimation under operational and abuse conditions. Appl Therm Eng. 2024;254:123895.

[7] Li K, Gao X, Peng S, Wang S, Zhang W, Liu P, et al. A comparative study on multidimensional signal evolution during thermal runaway of lithium-ion

batteries with various cathode materials. Energy. 2024;300:131560.
[8] Wang G, Ping P, Kong D, Peng R, He X, Zhang Y, et al. Advances and challenges in thermal runaway modeling of lithium-ion batteries. Innov. 2024;5(4).
[9] Wang C, Chen Y, Luan W, Li S, Yao Y, Chen H. Interpretable deep learning for accelerated fading recognition of lithium-ion batteries. ETransp. 2023;18:100281.
[10] Jiang Y, Liu Z, Kabirzadeh P, Wu Y, Li Y, Miljkovic N, Wang P. Multi-fidelity physics-informed convolutional neural network for heat map prediction of battery packs. Reliab Eng Syst Saf. 2025;256:110752.
[11] Naguib M, Kollmeyer P, Emadi A. Application of deep neural networks for lithium-ion battery surface temperature estimation under driving and fast charge conditions. IEEE Trans Transp Electrific. 2022;9(1):1153-1165.
[12] Karmakar A, Zhou H, Vishnugopi BS, Mukherjee PP. Thermal runaway propagation analytics and crosstalk in lithium-ion battery modules. Energy Technol. 2024;12(2):2300707.
[13] Zhang P, Chen H, Yang K, Lu Y, Huang Y. Accelerated computational strategies for multi-scale thermal runaway prediction models in Li-ion battery. Energy. 2024;305:132371.
[14] Shi C, Zhu D, Zhang L, Song S, Sheldon BW. Transfer learning prediction on lithium-ion battery heat release under thermal runaway conditions. Nano Res Energy. 2024;3(4).
[15] Cho G, Zhu D, Campbell JJ, Wang M. An LSTM-PINN hybrid method to estimate lithium-ion battery pack temperature. IEEE Access. 2022;10:100594-100604.
[16] Legala A, Li X. Hybrid data-based modeling for the prediction and diagnostics of Li-ion battery thermal behaviors. Energy AI. 2022;10:100194.
[17] Li H, et al. Immune multipath reliable transmission with fault tolerance in wireless sensor networks. In: Bio-inspired Computing–Theories and Applications: 11th International Conference, BIC-TA 2016, Xi'an, China, October 28–30, 2016, Revised Selected Papers, Part II. Singapore: Springer; 2016. p. 513–517.
[18] Zhao J, Han X, Ouyang M, Burke AF. Specialised deep neural networks for battery health prognostics: Opportunities and challenges. J Energy Chem. 2023;87:416–438.
[19] Grandhi, S. H., Al-Jawahry, H. M., Kumar, B. V., & Padhi, M. K. (2024, August). A quantum variational classifier for predictive maintenance and monitoring of battery health in electric vehicles. In 2024 International Conference on Intelligent Algorithms for Computational Intelligence Systems (IACIS) (pp. 1-4). IEEE.
[20] Ouyang N, Zhang W, Yin X, Li X, Xie Y, He H, Long Z. A data-driven method for predicting thermal runaway propagation of battery modules considering uncertain conditions. Energy. 2023;273:127168.
[21] Grandhi, S. H., Alabdeli, H., Lakshmanan, M., Soujanya, T., & Soni, M. (2024, August). A hybrid optimized model for battery management system in E-vehicles. In 2024 Second International Conference on Networks, Multimedia and Information Technology (NMITCON) (pp. 1-5). IEEE.
[22] Ding S, Dong C, Zhao T, Koh L, Bai X, Luo J. A meta-learning based multimodal neural network for multistep ahead battery thermal runaway forecasting. IEEE Trans Ind Inform. 2020;17(7):4503–4511.